HAL open science

Reconciling two alternative mechanisms behind bi-decadal variability in the North Atlantic

Pablo Ortega, Juliette Mignot, Didier Swingedouw, Florian Sévellec, Éric Guilyardi

To cite this version:

Pablo Ortega, Juliette Mignot, Didier Swingedouw, Florian Sévellec, Éric Guilyardi. Reconciling two alternative mechanisms behind bi-decadal variability in the North Atlantic. Progress in Oceanography, 2015, 137 (Part A), pp.237-249. 10.1016/j.pocean.2015.06.009 . hal-01176201

HAL Id: hal-01176201

https://hal.sorbonne-universite.fr/hal-01176201v1

Submitted on 16 Jul 2015

HAL is a multi-disciplinary open access archive for the deposit and dissemination of scientific research documents, whether they are published or not. The documents may come from teaching and research institutions in France or abroad, or from public or private research centers.

L'archive ouverte pluridisciplinaire **HAL**, est destinée au dépôt et à la diffusion de documents scientifiques de niveau recherche, publiés ou non, émanant des établissements d'enseignement et de recherche français ou étrangers, des laboratoires publics ou privés.

Reconciling two alternative mechanisms behind bi-decadal variability in the North Atlantic

Pablo Ortega (1), Juliette Mignot (1,2), Didier Swingedouw (3), Florian Sévellec (4), Eric Guilyardi (1,5)

[1]*LOCEAN Laboratory-IPSL, Sorbonne Universités (UPMC, Univ Paris 06)-CNRS-IRD-MNHN, 4 place Jussieu, F-75005 Paris, France*

[2]Climate and Environmental Physics and Oeschger Centre for Climate Change Research, University of Bern, Switzerland

[3]*EPOC, Université Bordeaux, Bordeaux, France*

[4]Ocean and Earth Science, National Oceanography Centre Southampton,University of Southampton, Southampton, UK

[5]*NCAS-Climate, University of Reading, UK*

Corresponding author:
Pablo Ortega *E-mail*: *pablo.ortega@locean-ipsl.upmc.fr*

MANUSCRIPT ACCEPTED IN PROGRESS IN OCEANOGRAPHY

Abstract:

Understanding the preferential timescales of variability in the North Atlantic, usually associated with the Atlantic meridional overturning circulation (AMOC), is essential for the prospects for decadal prediction. However, the wide variety of mechanisms proposed from the analysis of climate simulations, potentially dependent on the models themselves, has stimulated the debate of which processes take place in reality. One mechanism receiving increasing attention, identified both in idealised models and observations, is a westward propagation of subsurface buoyancy anomalies that impact the AMOC through a basin-scale intensification of the zonal density gradient, enhancing the northward transport *via* thermal wind balance. In this study, we revisit a control simulation from the Institut Pierre-Simon Laplace Coupled Model 5A (IPSL-CM5A), characterised by a strong AMOC periodicity at 20 years, previously explained by an

upper ocean-atmosphere-sea ice coupled mode driving convection activity south of Iceland. Our study shows that this mechanism interacts constructively with the basin mode propagation in the subsurface. This constructive feedback may explain why bi-decadal variability is so intense in this coupled model as compared to others.

1. Introduction

A growing body of studies reports dominant variability in the North Atlantic at the 20-30 and 50-70 year time scales, in models *(Delworth et al., 1993; Timmermann et al., 1998; Cheng et al., 2004; Dong & Sutton, 2005; Danabasoglu, 2008; Ortega et al., 2012; Escudier et al., 2013)*, as well as in observational *(Schlesinger & Ramankutty, 1994; Venegas & Mysak, 2000; Rayner et al., 2003; Frankcombe et al., 2010)* and proxy sources *(Gray et al., 2004; Sicre et al., 2008; Chylek et al., 2011; Cronin et al., 2014)*. Nevertheless, to date, no consistent explanation succeeds in providing a common coherent mechanism to any of these two preferential frequency bands.

One of the most challenging issues for decadal prediction is the identification of mechanisms with important impacts on climate. The AMOC is a key player for North Atlantic multidecadal variability; however, its ultimate drivers are not yet completely understood. Since the pioneering work of Delworth et al. (1993), characterizing an AMOC 50-year damped oscillation in an early version of the atmosphere-ocean coupled model of the Geophysical Fluid Dynamics Laboratory (GFDL), which resulted from an interplay between North Atlantic deep convection and salinity advection from southern latitudes, many other alternative mechanisms have been identified in other models. Even if many studies still support a leading role of convection on AMOC variability, the feedback processes and the time-scales involved are very diverse. Also, it is not always clear whether and how the AMOC adjust to changes in deep convection and deep water formation (Deshayes & Frankignoul, 2005).

A similar mechanism to the one described for the early version of the GFDL model has been identified by Dong & Sutton (2005) in the third Hadley Centre coupled Climate Model (HadCM3), but operating at a shorter timescale: ~25 years. Other studies (Danabasoglu, 2008; Ortega et al., 2012) using respectively the Community Climate System Model version 3 (CCSM3) and the coupled model European Centre Hamburg 4–Hamburg Ocean Primitive Equation–G (ECHO-G) link Labrador deep water formation and the North Atlantic Oscillation with preferential variability at 20 years. Both support a crucial role of the atmosphere through associated surface fluxes and wind-stress curl forcing. Kwon and Frankignoul (2014) have revisited the former CCSM3 simulation and propose an alternative ocean-only mode instead, where bi-decadal variability results from an interaction between the North Atlantic Current (NAC) and the equatorward deep return flow. Feedback mechanisms with the Intertropical Convergence Zone (ITCZ) can also produce centennial AMOC modulations, as observed first by Vellinga and Wu (2004) in HadCM3, and later on by Menary et al (2012) in other models. There are also internal ocean mechanisms that relate AMOC variability at long timescales [up to 80 years] to the export of freshwater anomalies from the Arctic into the Nordic (Jungclaus et al., 2005) and Labrador Seas (Hawkins & Sutton, 2007), respectively for the European Centre Hamburg Model version 5–Max Planck Institute Ocean Model (ECHAM5/MPI-OM) and HadCM3. More recently, Escudier et al. (2013) have shown that the East Greenland Current (EGC) intensity is paramount to explain the phase reversal of a bi-decadal ocean mode from the low-resolution version of the Institut Pierre-Simon Laplace Coupled Model 5A (hereafter IPSL-CM5A), involving surface salinity advection by the subpolar gyre as a driver of convective activity south of Iceland and subsequently of the AMOC. All these mechanisms are difficult to reconcile, as they might be model-dependent. One common aspect identified in several models is the modulation of the

AMOC and NAC strength by changes in upper ocean density anomalies at the western margin of the basin, an important region for the thermal wind relation (Tulloch & Marshall, 2012). The source region of these anomalies can however vary from one model to another, depending, for example, on the location of the main regions of convection.

One multidecadal mechanism consistently identified in idealized ocean models *(e.g. Colin de Verdière & Huck, 1999; Huck et al., 1999; te Raa & Dijkstra, 2002)* is related to the westward propagation of subsurface temperature anomalies across the North Atlantic basin. It will be hereafter referred to as *subsurface basin mode,* to acknowledge the importance of closed east and west boundaries to select the zonal wavenumbers, which set the timescale of the oscillation (Sévellec and Huck, 2015). Its link with the AMOC is explained by a thermal-wind driven interplay between the zonal and meridional overturning circulations *(te Raa & Dijkstra, 2002)*. This mechanism is also referred to as "thermal Rossby mode", because temperature anomalies propagate westwards across the mean temperature gradient, in the same way that Rossby waves do across the background potential vorticity gradient field. There exist evidence of a similar westward propagation in North Atlantic observations of sea-level height *(e.g. Tulloch et al., 2009; Vianna & Menezes, 2013)*, subsurface *(Frankcombe et al., 2008)*, and sea surface temperature *(Feng & Dijkstra, 2014),* with comparable basin-crossing times as for the *subsurface basin mode.* Despite this consistency between observations, modeling and theory, it is still under debate whether this interdecadal AMOC variability is excited by the atmosphere or maintained by pure ocean dynamics. Whereas *Colin de Verdière and Huck (1999)* and *Sévellec and Huck (2015)* suggest that it can be internally forced by large-scale baroclinic instabilities, *Killworth and Blundell (2007)* and *Sévellec et al (2009)* advocate for the need of an external energy source, either a local wind

forcing or a buoyancy exchange (*e.g.* heat or freshwater fluxes). Recently, *Sévellec and Fedorov (2013)* have demonstrated that this oscillation appears as the least damped multidecadal oscillatory mode in OPA (*Océan PArallélisé*), the oceanic component of the IPSL-CM5A model. In their study, the AMOC exhibits a peak of preferential variability at 20 years. The damped nature of this mode could point to a necessary role of the atmosphere to sustain the AMOC oscillation, although this feature could be model dependent. It remains therefore unclear whether this potentially damped internal ocean mode will be present when the ocean model OPA is coupled to an atmospheric model. Another question is whether this mode is compatible with the convection-driven AMOC mechanisms described above.

These two intriguing questions can be addressed within the IPSL-CM5A model. Here we revisit the same coupled control simulation analysed in *Escudier et al. (2013)* and demonstrate that their upper ocean-atmosphere-sea ice coupled mechanism coexists with a multidecadal subsurface basin mode like the one described in *Sévellec and Fedorov (2013)* for the ocean component alone. Hence, new questions will be also tackled: Are both modes developing independently, and interact constructively or destructively over time? Otherwise, is one driving the other? Or are both coupled to each other? We will show that both oscillations are intrinsically linked, as two different expressions of a larger coupled mechanism.

The paper is organised as follows. The model and the coupled run are presented in Section 2. This section also includes a detailed description of the two mechanisms investigated. Section 3 assesses the presence of the subsurface basin mode in the coupled model, and Section 4 investigates the potential feedbacks between the two *a priori* different modes. Conclusions and a discussion of implications are included in section 5.

2. Model and theoretical basis

2.1 The IPSL-CM5A model

The analysis is based on a 1000-year long control preindustrial run with the IPSL-CM5A model, performed within the framework of the fifth Coupled Model Intercomparison Project (CMIP5). It uses the LMDZ5A (Laboratoire de Météorologie Dynamique-Zoom version 5A) atmospheric circulation model *(Hourdin et al. 2013*), under a regular 96 x 96 point horizontal grid (*i.e.* 3.75° x 1.875°) with 39 levels in the vertical. The oceanic component is the Nucleus for European Modelling of the Ocean (NEMO) version 3.2 (*Madec, 2008*). It includes the OPA9 ocean circulation model, coupled with the Louvain-la-Neuve (LIM2) sea-ice model version 2 *(Fichefet & Maqueda, 1997*) and the biogeochemical module PISCES (for Pelagic Interaction Scheme for Carbon & Ecosystem Studies; *Aumont & Bopp, 2006*). The ocean component includes 31 vertical levels, 15 of them in the upper 150 m and has an irregular horizontal grid of 182 x 149 points, characterized by a nominal resolution of 2° with an enhancement over the Arctic, the subpolar North Atlantic and near the Equator. Further details on the model configuration, its different components and the boundary conditions imposed to run the control simulation can be found in *Dufresne et al. (2013)* and references therein. Other studies describing the components and various different aspects of the model performance are compiled in a special issue of Climate Dynamics (http://link.springer.com/journal/382/40/9/). In particular, the performance of the oceanic component in the coupled model configuration is assessed in *Mignot et al. (2013).*

2.2 The upper ocean-atmosphere-sea ice coupled mode

In a first analysis of the control IPSL-CM5A simulation, *Escudier et al. (2013)* identified a strong 20-year periodicity in several key variables across the North Atlantic basin.

This common variability is explained through a coupled atmosphere-ocean mode mainly acting in the upper ocean (Figure 1). The 20-year cycle starts, for example, with a deceleration of the EGC, which reduces the export of fresh and cold polar waters through the Denmark Strait. This generates within 3 years anomalous warm and salty upper waters in the Labrador Sea that are advected eastward by the subpolar gyre, and reach, in 5 years time, a region of convection located South of Iceland, and 2 years after the Nordic Seas. The region South of Iceland is the major area for deep convection in the model, but its role is less important in the real world (Marshall and Schott, 1999). This model bias should be kept in mind when assessing the realism of this mode. In the Nordic Seas, the warm temperature anomalies contribute to reduce the sea-ice extent, and produce a cyclonic atmospheric circulation response, leading to an intensification of the Ekman transport over the Denmark Strait, and ultimately of the EGC strength. This atmospheric link, although rather weak, provides the necessary feedback for the phase reversal 10 years after the initial EGC weakening. The EGC phase reversal is also fostered by a reduction in the sea ice cover over the Denmark Strait region, which increases the momentum exchange between the atmosphere and the ocean. The second part of the cycle evolves similarly, this time with fresh and cold surface waters from the Arctic being advected along the subpolar gyre, and giving rise 7 years later to positive sea ice extent and negative SLP anomalies in the Nordic Seas. The AMOC does not seem to play an active role in this mechanism. Nevertheless, it does respond passively, with 8-9 years lag, to changes in deep convection in the region South of Iceland. The reasons for this particular lagged response were not addressed in the original study of Escudier et al (2013) and are further explored in the present study.

Due to the predominant role of surface variables in this bi-decadal mode, the IPSL-CM5A model has a great potential for AMOC initialization and decadal prediction.

Indeed, two perfect model analyses by *Persechino et al. (2013)* and *Servonnat et al. (2015)* have respectively shown that, in the model, the AMOC has an average potential predictability of 8 years and can be successfully recovered, by applying a nudging to sea surface temperature and salinity fields, that is able to initialize its major precursors (*e.g.* EGC, convection South of Iceland). Likewise, *Swingedouw et al. (2013)* argued that this advective surface mechanism may explain two of the observed Great Salinity Anomalies occurring in the 1970s and 1990s *(Belkin et al., 1998),* which in the model follow an excitation of this 20-year cycle by Mt Agung eruption.

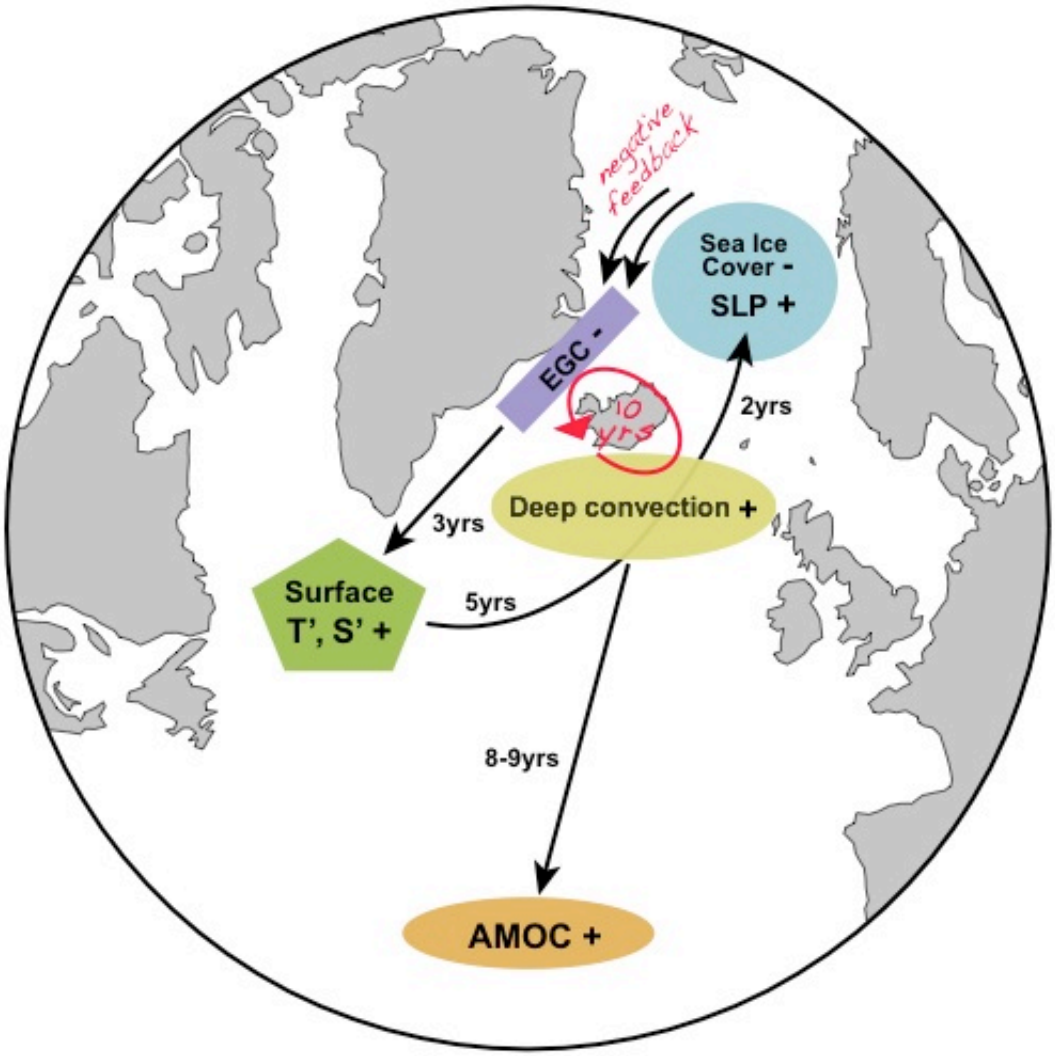

Figure 1: Schematic representation of the advective mechanism, modified from Figure 13 in Escudier et al. (2013). Estimated time-lags are indicated along the arrows. The corresponding sign of the anomalies appears next to each variable.

2.3 The subsurface basin mode

This multidecadal oscillatory mechanism has been identified in several idealized models and theoretical studies (e.g. Colin de Verdière & Huck, 1999; Huck et al. 1999; Te Raa & Dijkstra, 2002; Sévellec & Huck, 2015), as well as in the linearized version of the ocean component of IPSL-CM5A, as described in *Sévellec and Fedorov (2013).* It is characterised by a large-scale westward propagation of subsurface density anomalies, typical of large-scale baroclinic Rossby waves *(Colin de Verdière & Huck, 1999)*. This westward propagation can occur even under the presence of a dominant eastward mean flow, due to the contribution of two additional terms that oppose the *mean zonal advection*: the *geostrophic self-advection* and the *ß-effect*. *Geostrophic self-advection,* initially characterised within the paradigm of the non-Doppler shift effect *(e.g. Rossby, 1939; Held, 1983; Killworth et al., 1997)*, is triggered by a local density perturbation (either thermal or haline) embedded along a mean meridional density gradient (normally increasing northward). For instance, positive local density anomalies produce a geostrophic cyclonic response, bringing denser waters from the south to its western flank, and lighter waters from the north to its eastern flank, thus leading to an effective propagation to the west. Note that negative density anomalies also move westward, because they induce an anticyclonic response instead. The other term, the *ß-effect,* is typical of long non-dispersive baroclinic Rossby waves. It works similarly to self-advection, but relies on the variation of the Coriolis parameter with latitude (instead of the isopycnal depth). In the Northern Hemisphere, the *ß-effect* is always positive and thereby contributes to a westward propagation. The combination of the *mean zonal flow*, the *geostrophic self-advection* and the *ß-effect* determines the full speed of the propagation (*Sévellec and Fedorov, 2013*).

The multidecadal oscillatory mode can be described following four major phases (two of them shown in Figure 2). In Phase I, a large-scale positive density anomaly appears in

the middle of the basin in the North Atlantic, and propagates westward consistently with the self-advective mechanism. The propagation eventually leads to Phase II, in which a zonal density gradient is established, with denser waters at the west and lighter waters at the east of the Atlantic basin. This configuration strengthens the AMOC *via* thermal wind balance. As a result of the associated enhanced downwelling in the North Atlantic, the sign of the initial density anomalies is reversed a few years later. To complete a full oscillation cycle, the two previous phases are followed by their two corresponding opposite phases: negative density anomalies in the middle of the basin propagating westward; and a weakening in the AMOC strength, caused by a reversal of the zonal gradient in Phase II.

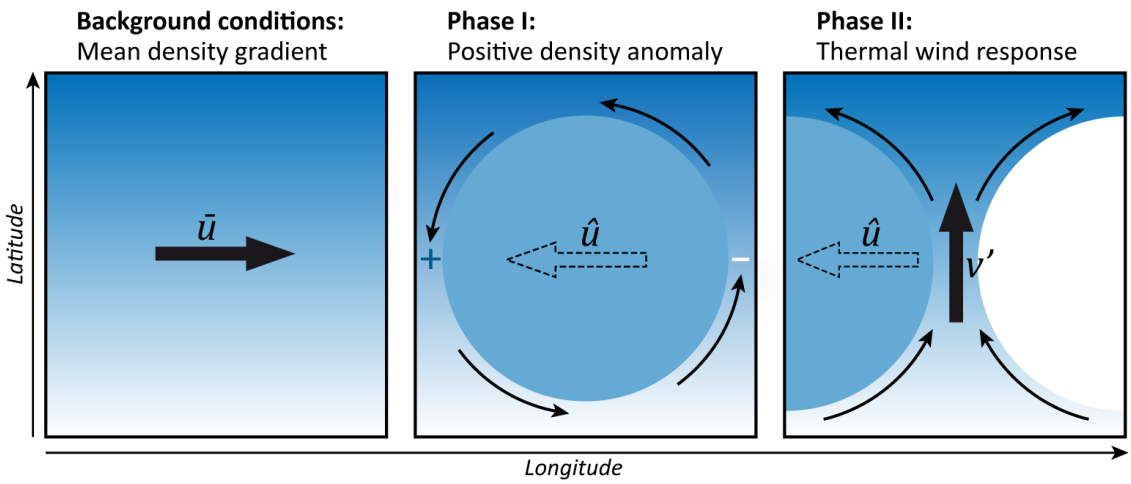

Figure 2: Schematic of the multidecadal oscillatory mode modified from Figure 4 of *Sévellec and Fedorov (2013)*. The background colour degradation represents the mean density distribution, with lighter waters in white and heavier waters in blue. (Left) Background conditions correspond to a mean meridional density gradient and an eastward mean zonal velocity $\bar{u}$. (Middle) In the first phase, positive density anomalies appear in the middle of the basin and generate a geostrophic cyclonic flow that induces a westward propagation. (Right) In phase II the original positive density anomaly has reached the western boundary, and negative anomalies have emerged in the east. This zonal density gradient intensifies the northward surface flow v' through thermal wind balance.

The basin mode is fundamentally linked to the existence of zonal boundaries, which allow the reemergence of density anomalies at the eastern boundary, opposite in sign to the anomalies reaching the western boundary. In OPA9, this reemergence is consistent with a fast adjustment by Kelvin waves propagating southward along the western boundary, through the equator, and subsequently northward along the eastern

boundary (Sévellec and Fedorov, 2013), as previously described in Johnson and Marshall (2002).

2.4 Computation of the thermal wind transport.

As described above, the effect of the subsurface basin mode on the AMOC arises through a modulation of the west-to-east density gradient, which triggers a meridional thermal wind response. The northward thermal wind transport at a particular depth z' is calculated using the following decomposition:

$$\psi_{tw}(z) = \int_{x_w}^{x_e} dx \int_{-H}^{z} (\tilde{v} - v_0) dz' \qquad [1]$$

where x, ψ_{tw}, H, x_e, x_w, $\tilde{v}$ and v_0 represent respectively the zonal coordinate, the thermal-wind contribution to the meridional streamfunction, the total ocean depth, the longitude of the eastern and western boundaries, the meridional velocity associated with the zonal density gradient and a correction term introduced to guarantee mass conservation without affecting the vertical shear.

The meridional velocity $\tilde{v}$ is calculated from the zonal density gradient as follows:

$$\tilde{v}(z) = \frac{g}{\rho_0 f} \int_{-H}^{z} \frac{1}{L(z)} (\rho_w - \rho_e) dz' \qquad [2]$$

where z, g, ρ_0, ρ_e, ρ_w, f, L and H are respectively the vertical coordinate, the gravitational acceleration, a reference density, the density at the eastern and western boundaries, the Coriolis parameter, the basin width, and the bottom of the ocean. Note that, in essence, this decomposition is based on the geostrophic balance, the hydrostatic approximation and mass conservation. It was derived and tested in depth in *Hirschi and Marotzke (2007)*, and has been used in an operational context for monitoring AMOC variations within the RAPID array (*Cunningham et al., 2007*).

2.5 Analysis and statistical assessment

Our study is mainly based on the statistical links of different indices among themselves and also with other large-scale climate fields. All data correspond to annual means, and anomalies are calculated with respect to the simulation long-term mean (*i.e.* 1000 years). Statistical significance of all the regression and correlation coefficients is assessed following a two-tailed Student's *t* test. Sample size is corrected by taking into account the series autocorrelation, thus reducing the sample degrees of freedom to its effective value (*Bretherton et al., 1999*).

3. Characterizing the subsurface basin mode propagation in IPSL-CM5A

The climatological maximum of the AMOC streamfunction is approximately 10 Sv, well below the range of observational estimates (*Ganachaud & Wunsch, 2000; Talley et al., 2003*). This is probably caused by a misrepresentation of Labrador convection in the model, and an underestimation of the outflows from the Nordic Seas (*Escudier et al., 2013*).

To highlight the 20-year cycle in the AMOC, we define a meridional overturning index as the maximum streamfunction value at 48°N (MOI-48N) and remove the Ekman transport contribution. This is the latitude where the climatological means of both the full AMOC streamfunction and the thermal wind transport become maximum (Figure 3). Note that the differences between both quantities in Figure 3 relate to the contribution of the Ekman transport and to the approximations considered to derive Equation 1. Despite the climatological differences, more important at depth, both quantities show rather similar variability in the vicinity of the climatological maximum. The MOI-48N and an equivalent index for the thermal wind transport are strongly correlated, with a correlation coefficient *r* of 0.8 (significant at the 95% confidence level).

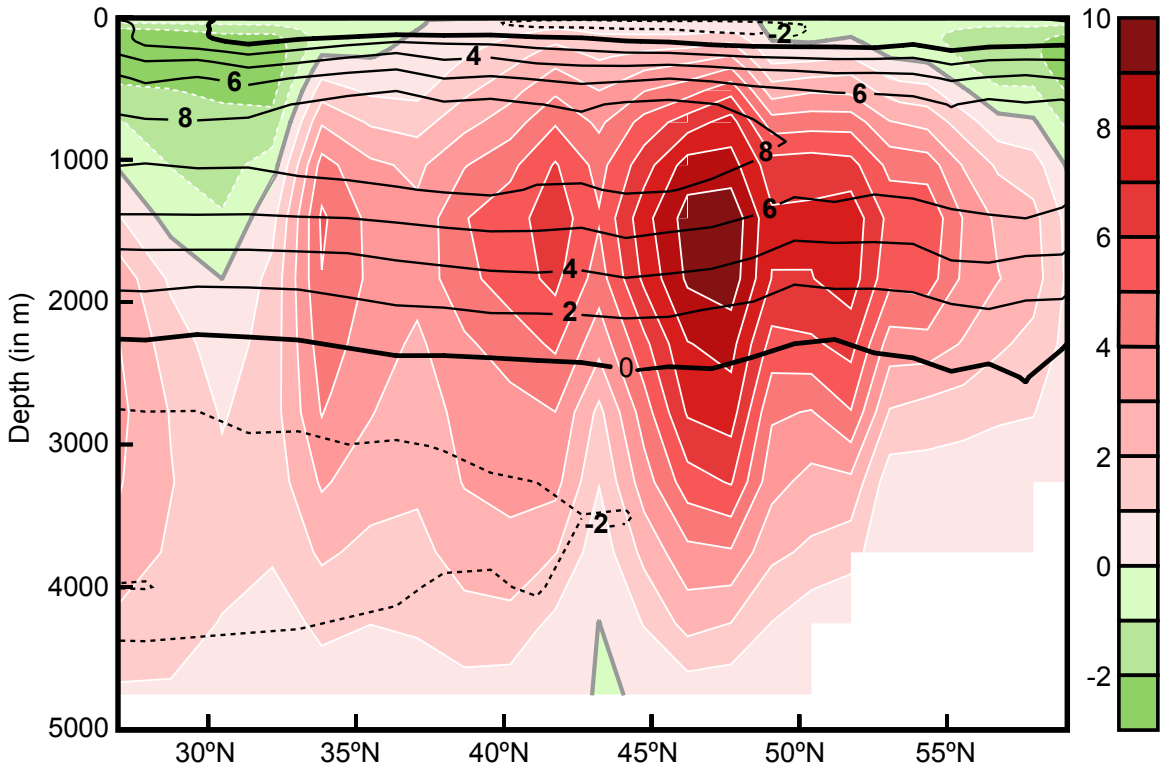

Figure 3: Long-term mean of the northward thermal wind transport in the North Atlantic (shaded, in Sv) as computed from the density fields at the coastal boundaries following Equation 1. The mean Atlantic meridional overturning circulation streamfunction (also including the Ekman transport) is superposed in contours (also in Sv).

Figure 4 shows in-phase correlations between the MOI-48N index and the density profile at the same latitude. From Equation 2, increased northward thermal wind transport is only possible when $\rho_w > \rho_e$. This implies that the MOI-48N can be interpreted in terms of the thermal wind only below 300m, as the zonal gradient is reversed above this level. More precisely, the strongest positive west-to-east density gradient is established between 300 and 1000 m, enhanced simultaneously by denser waters at the west and lighter at the east side of the basin. The climatological density gradient is also stronger at these subsurface levels (black contours in Fig. 4).

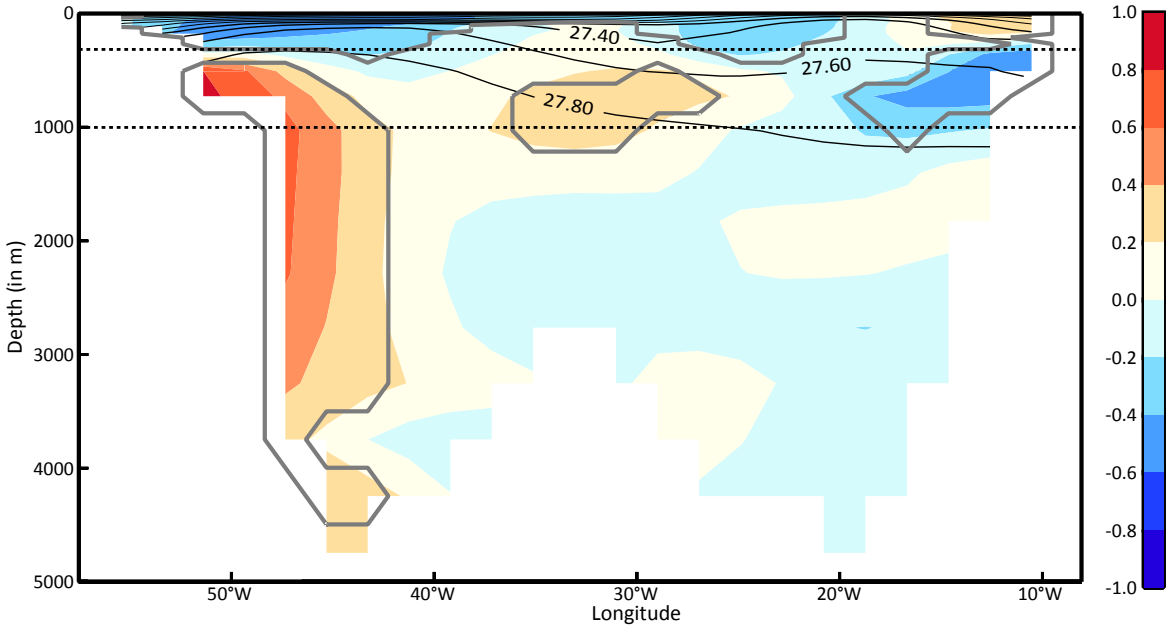

Figure 4: Correlation profile (depth-longitude) between the MOI-48N and local density (referenced to the sea surface) at the same latitude. Significant values at the 95% confidence level are enclosed by the thick grey contours. Black thin contours describe the background density stratification in contour intervals of 0.2 kg/m³. Horizontal dotted lines delimit the levels at which the ρ_{west} - ρ_{east} gradient is strongest.

As expected from Figure 4, the spatial correlations between MOI-48N and the vertically averaged subsurface density fields (300-1000m, Figure 5a) are consistent with a basin-wide northward thermal wind response. Strong positive correlations appear all along the western coast of North America, with maximum values near the Labrador Sea and east of Nova Scotia. Negative correlations are observed in the convection region south of Iceland (green lines in Figure 5) and near the coasts of France and Spain. A rather different picture emerges for the upper ocean (Figure 5b), more characterized by a north-south dipole at subpolar latitudes, probably due to other contributions than the thermal wind. The advective mechanism discussed in *Escudier et al. (2013)* has in particular been shown to exhibit maximum signals at these levels. All of the above suggests that the two modes might be operating at two different depth ranges.

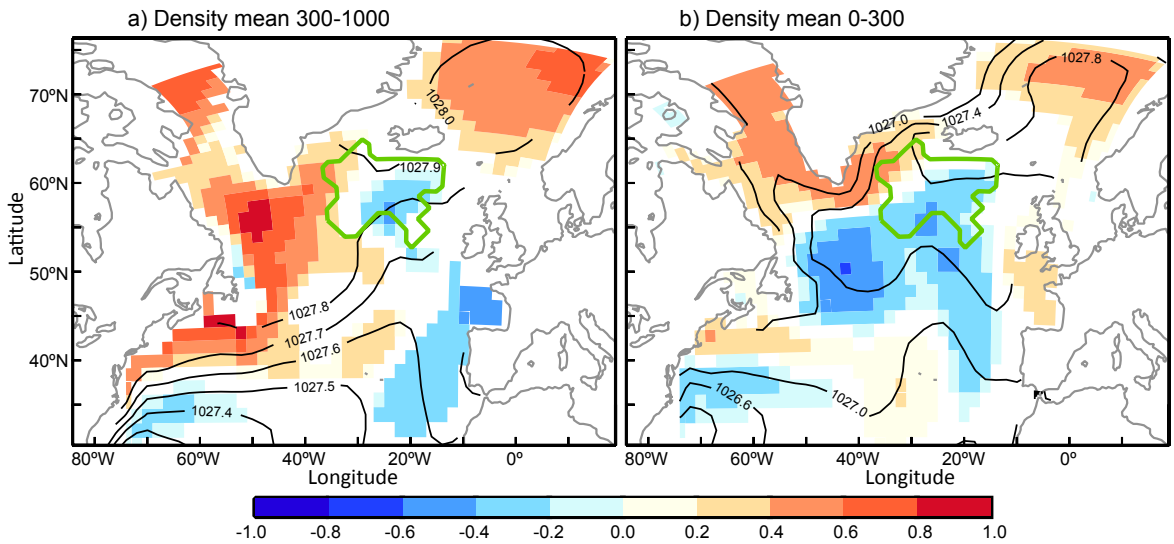

Figure 5: Correlation maps between the MOI-48N index and the vertically averaged density between: a) 300-1000m and b) 0-300m. Only those correlation coefficients significant at the 95% confidence level are shown. The background density field is represented in black contours. The green thick contour line encloses the region of convection South of Iceland.

Now that the optimal depths and regions contributing to the intensification of the northward thermal wind transport are well constrained, we can verify whether the positive density anomalies at the western side of the basin have propagated from the east, as it would be expected if the westward propagation from the subsurface basin mode was present. This is addressed in Figure 6. The first two columns represent the regressions at different lags between the standardized MOI-48N index and the subsurface (*i.e.* 300-1000m) density averaged over two different latitude ranges. In the subpolar region (*i.e.* 34 to 65°N) positive density anomalies are indeed formed near 30°W and propagate slowly to the west reaching the coast about 5 years later, when the AMOC becomes maximum (lag zero). This evolution is coherent with the multidecadal subsurface basin mode. However, no propagation of anomalies of opposite sign reaching the western side of the basin is observed at subsequent lags. This latitudinal band is the same where *Sévellec and Fedorov* (2013) identified their westward propagation. Yet, they observed it in the upper ocean, where our model presents an eastward propagation (not shown) and where the advective mechanism of *Escudier et al. (2013)* mainly takes place. When the analysis is restrained to the northernmost part

of the region, where the zonal density gradient is strongest (*i.e.* 50-65°N), the westward propagation is more clear. The Hovmöller in Figure 6b shows how positive and negative density anomalies move westwards with bi-decadal periodicity (T=20 years), in accordance with the changes in the AMOC. These features remain coherent for density anomalies integrated down to 3000 m (not shown). By contrast, no basin-wide westward propagation of density anomalies is observed at the surface levels (Figure 6c).

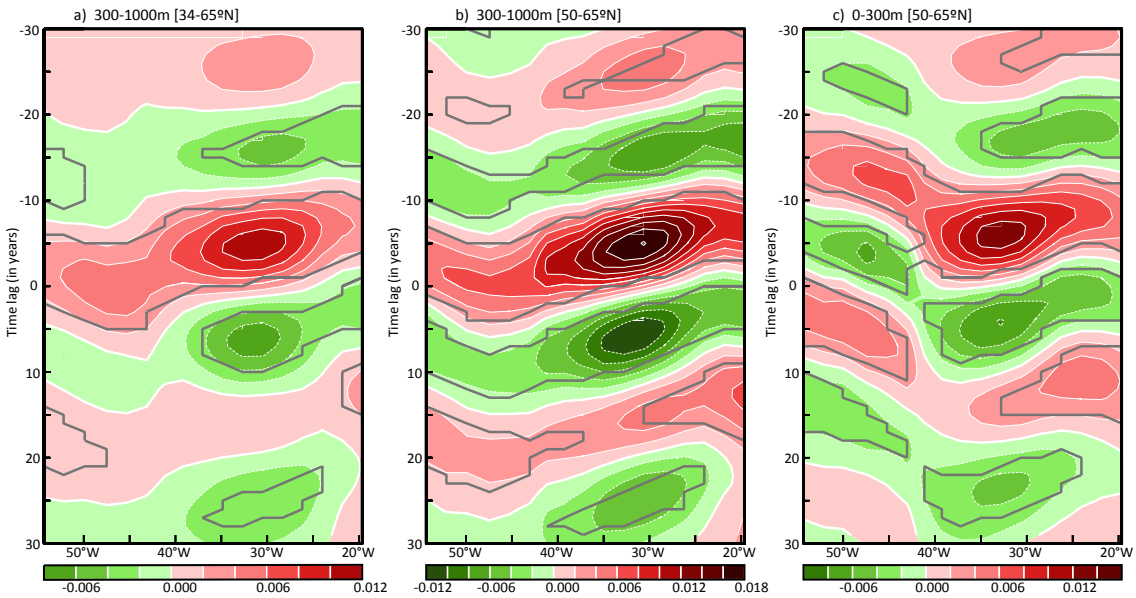

Figure 6: Hovmöller plot (Time lag vs. Longitude) of the regression (in kg/m^3) between the standardized MOI-48N and the meridionally averaged density anomalies at: a) 300-1000m in the latitude band 34-65°N; b) 300-1000m in 50-65°N and c) 0-300m in 50-65°N. Significance is assessed as in Figure 4.

To determine the role of the mean zonal flow in explaining the propagation, the mean zonal velocities in the North Atlantic are compared qualitatively to the evolution of density anomalies (Figure 7), represented by the correlation contours of r=±0.5 between the MOI-48N and the vertically averaged density fields at different lags. In the upper ocean (Figure 7a), where the advective mechanism is at play, correlation contours describe a loop across the subpolar gyre as the AMOC strengthens (lags -10 to 0) and weakens (lags 0 to 6), with an excursion of anomalies into the Nordic Seas. Westward advection is only observed in the northern subpolar gyre and is almost exclusively confined to the EGC pathway, whereas eastward advection only occurs in

the south, in a region with predominant mean eastward currents. All of this supports the major role of the mean subpolar gyre currents already described in *Escudier et al. (2013)*. A somewhat different picture is found for the subsurface levels (Figure 7b), where mean currents are comparably weaker. Positive density anomalies start at lag -8 in the region south of Iceland and move westward across a wide latitudinal range (~56-67°N), including areas of positive (*i.e.* eastward) mean zonal velocities. This is possible due to the contribution of the *geostrophic self-advection* and *β-effect* terms described in Section 2.3, two key features of the subsurface basin mode. Note that, as expected, the propagation is faster in the EGC region, where mean zonal velocities are negative. These fast-propagating anomalies reach the western Greenland Sea at lag -6, and feed the Labrador Sea Current going south along the coast. The presence of this outflow is hinted by the eastward propagating anomalies from 55 to 50°W in Figure 6b. At lag -2, the density anomalies from the Labrador Current merge back with the anomalies propagating slowly outside of the EGC region, reaching the Newfoundland coast at this stage. In the immediate subsequent lags, there is a fast adjustment along the western boundary that strengthens the zonal density gradient and thus the AMOC. Note the appearance at lag 2 of negative correlation contours in the region of convection south of Iceland, also propagating slowly to the west outside of the EGC region, consistently with the oscillatory basin mode.

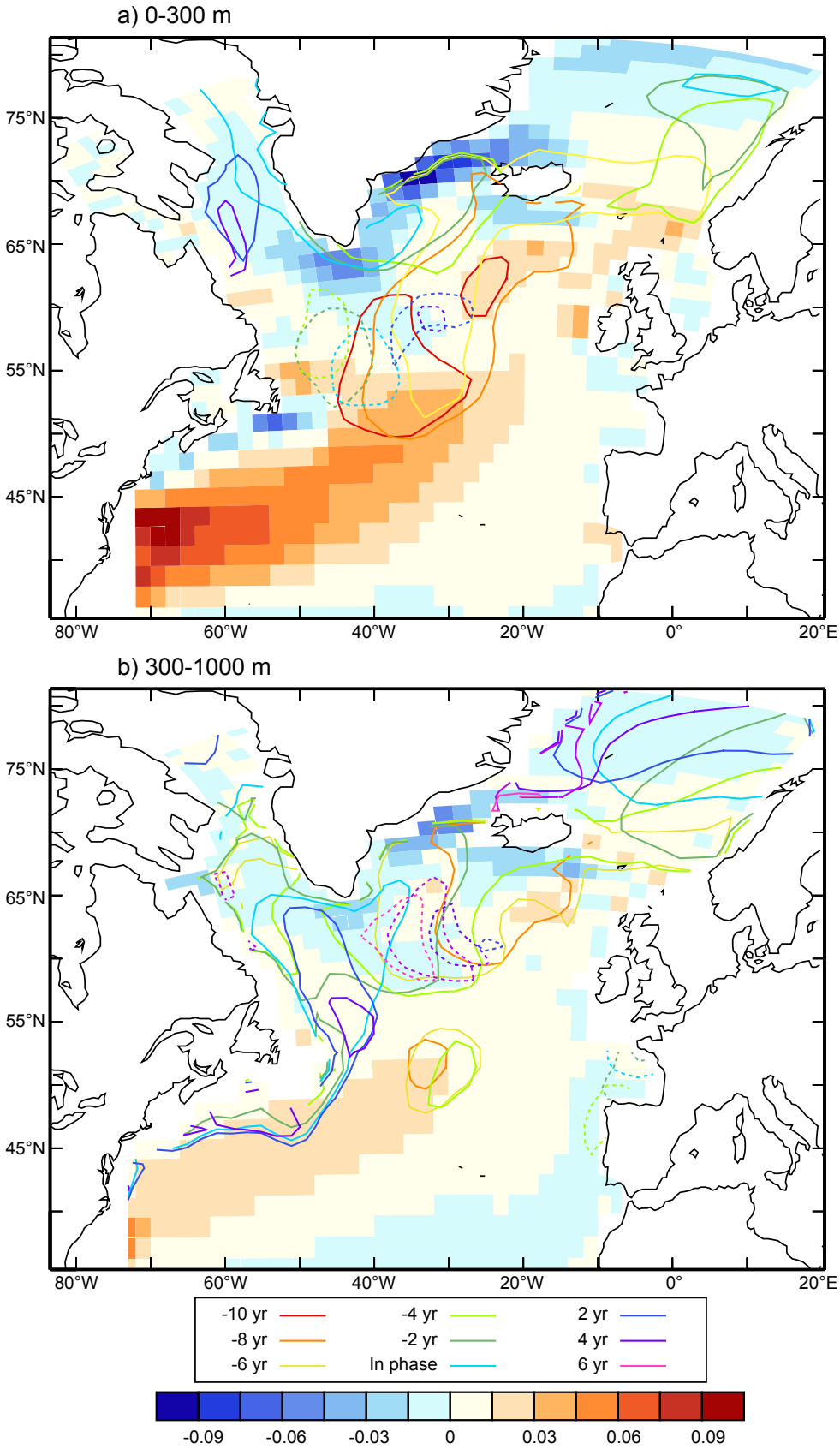

Figure 7: Vertically averaged zonal velocities (shaded, in m/s) in the levels: a) 0-300 m; b) 300-1000 m. The colored solid (dotted) contours represent the correlation contours of r=0.5 (r=-0.5) between the MOI-48N index and the vertically averaged density fields at different lead/lag times.

Further evidence of the basin mode propagation is provided in Figure 8a, showing the lead-lag regressions of the normalized MOI-48N with the vertically averaged density and velocity anomalies between 300 and 1000m. The first panel corresponds to a weak AMOC situation (-$T/2$; *i.e.* 10 years before the MOI-48N peaks), and shows a negative zonal density gradient ($\rho_{west} < \rho_{east}$) leading to a reduced northward transport *via* thermal wind balance. South of Iceland and north of 50°N there is a positive cell of density anomalies, also present in the upper layer (Figure 8b), generating by geostrophy a cyclonic flow response similar to the one described in *Sévellec and Fedorov (2013)*. This cyclonic response, through an interaction with the background density field (Figure 5, black contours), also contributes to the westward displacement. The *self-advection* term is higher in the regions where the south-to-north background density gradient is stronger, and can thereby compensate the eastward *mean zonal velocities* at the eastern side of the basin (Figure 7b). Thus, both contributions along with the *ß-effect* – of smaller amplitude than them but by definition always negative – can account together for an effective basin-wide westward propagation of the initial density anomalies. Indeed, at lag $-T/4$ the cyclonic cell is visibly displaced to the west, growing also in strength, notably along the Greenland coast. Note that at this stage the cyclonic cell extends also into the upper ocean (Figure 8b), where it intensifies the southward transport through the Denmark Strait, and therefore also the EGC strength. This link will be discussed in more detail in section 4.2. Strengthened AMOC situations (lag zero) set up when the positive anomalies have reached the Labrador coast and new negative anomalies (inducing this time an anticyclonic geostrophic response) are formed south of Iceland, thus reversing the initial zonal gradient and intensifying the northward transport through thermal wind balance. These negative density anomalies appear as a result of a reduction in convection following the arrival of negative upper density

anomalies from the Denmark Strait and Labrador regions (Figure 8, lags $-T/4$ and $-T/2$). For the positive lags (AMOC leading) $T/4$ and $T/2$ the opposite phase of the propagation takes place, this time with the negative density anomalies moving eastward in response to the associated anticyclonic flow bringing lighter waters into the west (coming from southern regions) and denser waters into the eastern flank (advected from the north).

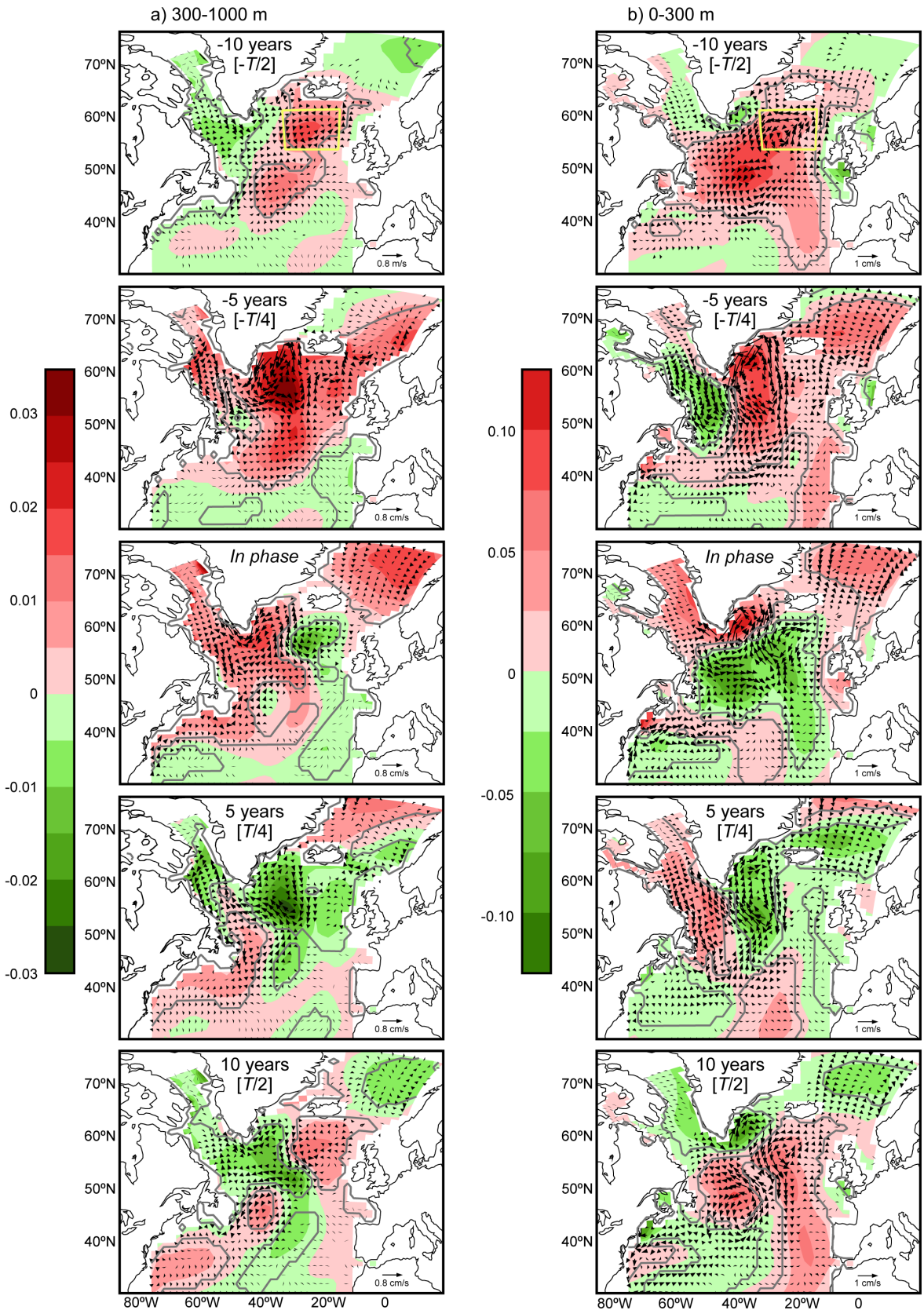

Figure 8: Time-lag regressions between the normalised MOI-48N index and both the vertically averaged density (shaded) and ocean velocity (vectors) anomalies in: a) 300-1000 m layer; b) 0-300 m layer. The lag is written in fractions of the period T (20 years). Significance is assessed as in Figure 4. The yellow box encloses the region where the index $\rho_{\text{NE-Atl}}$ is defined.

The balance of evidence presented here is thus consistent with the existence of a multidecadal basin mode in subsurface (300-1000m) linked to the variability of the AMOC. Furthermore, this mechanism operates at a similar timescale and in the same basin as the upper-ocean (0-300m) advection mechanism from *Escudier et al (2013)*. We now assess whether both mechanisms are independent, or interact with each other.

4. Interactions between the two bi-decadal modes

Given that both mechanisms vary at similar timescales and share several dynamical components, our working hypothesis is that both are coupled. There are two key quantities that could explain a link between the two modes: *deep convection* and the *EGC*.

4.1 From the upper ocean advective mechanism to the subsurface basin mode: the role of convection

The most evident link is ocean convection, because it connects the upper and the deeper ocean. Indeed, winter convection enhances oceanic heat release to the atmosphere, resulting in a net cooling and densification of the water column *(Swingedouw et al., 2007)*. In the coupled model, the convection region located south of Iceland (Figure 5) is the one showing strongest correlations with the AMOC (Escudier et al., 2013). Its variability is driven by anomalies in upper ocean salinity, which are built up in the Labrador Sea and advected eastward by the subpolar gyre. The arrival of positive salinity anomalies coincides with minimum values in the AMOC strength, a situation that weakens the meridional heat transport and gradually cools and densifies the upper layers in the North Atlantic. This effect of the AMOC on the vertical density structure in the convection region is illustrated in Figure 9. The MOI-48N is anticorrelated with density anomalies near the surface (mostly thermally driven), but also directly correlated with salinity-driven density anomalies at depth (Figure 9). Thus, weakened

AMOC situations reduce the vertical stratification, and contribute to facilitate deep convection when the positive surface salinity anomalies arrive. Following the increases in convection south of Iceland, anomalously dense waters are formed from the surface down to 2000 m depth (Figure 10), thus including the depth range where the basin mode propagation is observed. These are most probably the same density anomalies observed at lag -*T/2* in the northeast Atlantic (NE-Atl, yellow box in Figure 8), both in the upper (0-300) and intermediate (300-1000m) levels, and propagating westward in response to the induced anomalous cyclonic flow. This is supported by Figure 11a, showing that upper 1000m density anomalies in the northeast Atlantic box ($\rho_{NE\text{-}Atl}$) are highly correlated with mixed layer depth changes in the region south of Iceland ($MLD_{S\text{-}Ice}$; green contours in Figure 5). These anomalies lead the changes in the AMOC by about 8 years, which is the time they require to reach the western coast, enhance the zonal density gradient and thus increase the meridional thermal wind transport, as demonstrated by *Sévellec and Fedorov (2015)*. It is therefore through a stimulation of subsurface basin mode that the advective mechanism at the surface, and ultimately convection, comes to impact the variability of the AMOC several years after. Following *Sévellec and Fedorov (2015)* we have been able to provide a mechanistic explanation to the long delay between convection south of Iceland and the AMOC response previously reported in *Escudier et al. (2013)*.

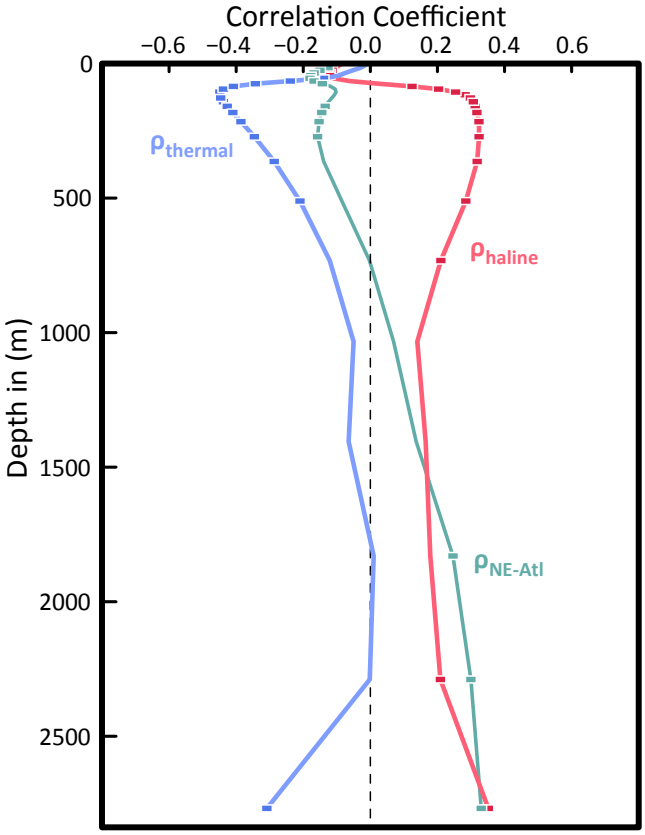

Figure 9: Vertical profile of the correlations between the MOI-48N index and density anomalies in the region of convection in the eastern North Atlantic (enclosed by the green contour in Figure 5). Both the full density and the related thermal and haline contributions are shown for comparison. Significant values at the 95% confidence level are highlighted with dots.

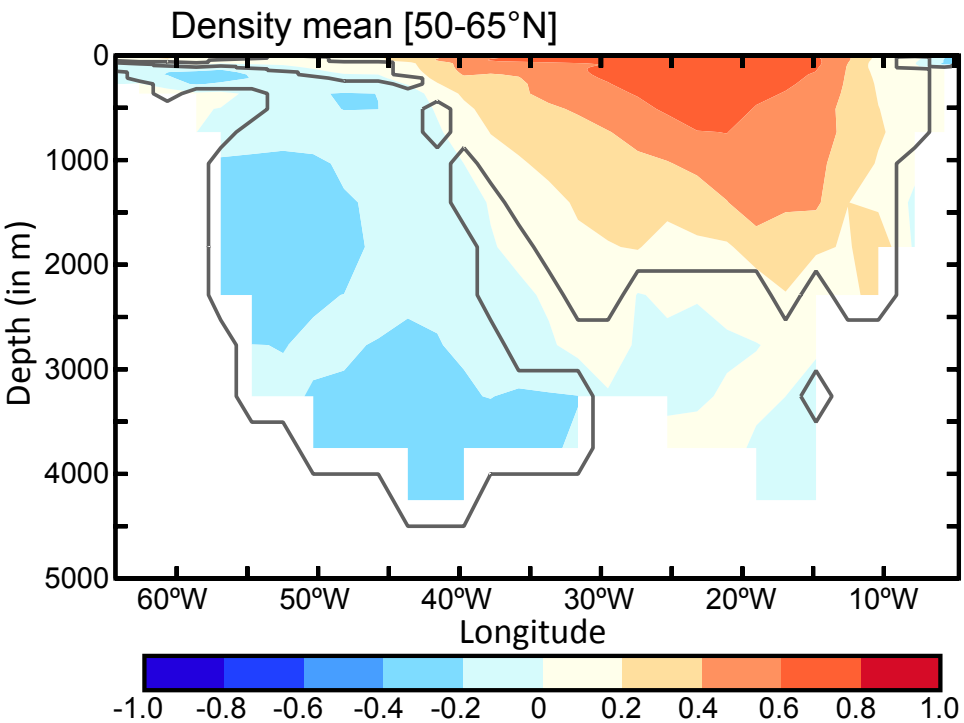

Figure 10: Correlation profile (longitude-depth) between an index of North Atlantic convection (region enclosed by the green contour in Figure 5) and the latitudinally averaged densities between 50-65°N. The index of convection is defined as the annual mixed layer depth mean in the region. Significance is assessed as in Figure 4.

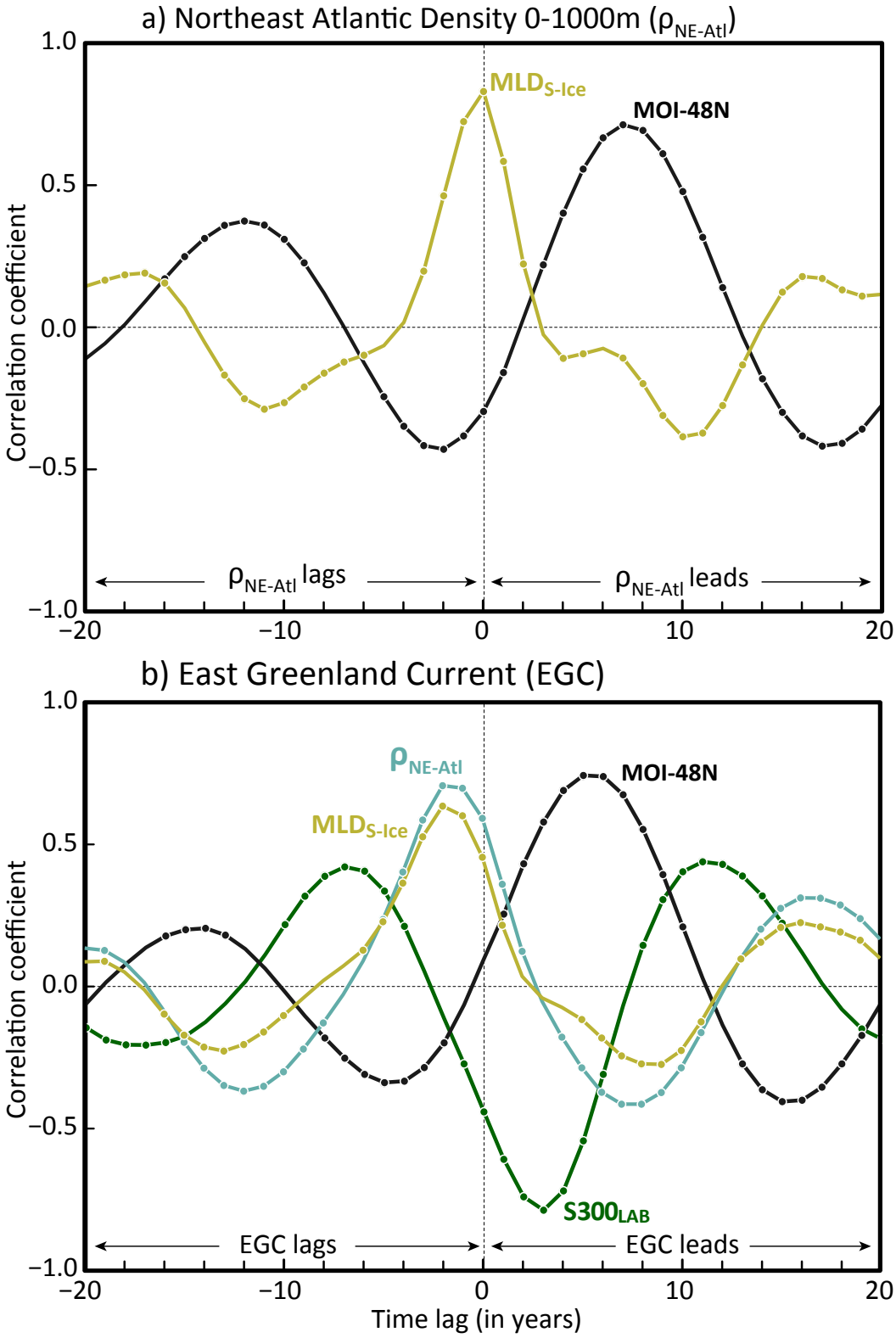

Figure 11: Lead-lag time correlation plot of several indices with: a) Northeast Atlantic density in the upper 1000m and b) the East Greenland Current intensity. Significant values at the 95% confidence level are highlighted with dots.

4.2 From the subsurface basin mode to the advective mechanism in the upper ocean: the role of the EGC

In order to understand whether and how the subsurface basin mode feeds back onto the subpolar-gyre advective mode at the surface, we focus on the EGC *(cf. Escudier et al., 2013)*. Indeed, this upper-ocean current, linking the Arctic waters with the subpolar gyre, is essential to explain the phase reversal of the salinity anomalies advected by the subpolar gyre in the advective mechanism. Here, we use the same definition as in *Escudier et al. (2013)*: the EGC is calculated as the outflow of waters through the Denmark Strait with mean salinity values lower than 34 psu. These are localized in the upper 200 m near the Greenland coast. In *Escudier et al. (2013),* EGC strengthenings were explained by a decrease in sea-ice cover in the Nordic Seas, producing an anomalous atmospheric cyclonic response that subsequently intensified Ekman transport through the Denmark Strait. This link, even if physically consistent, was found in that study to be somewhat weak. We revisit this interpretation under our new framework, in which the subsurface basin mode propagation is also at play. Figure 8 already showed that at the lag -$T/4$ (*i.e.* 5 years before an AMOC peak), the anomalous cyclonic cell, present both in the surface and the subsurface, is located near the Greenland coast, with a particularly intense southward transport branch at its western flank. This explains why EGC variability is strongly linked with the appearance, 5 years before (although with maximum correlation for a 2-year lead time), of the positive density anomalies in the northeast Atlantic (Figure 11b), which was shown before to be associated with increased convection. This EGC change, fueled by the anomalous cyclonic cell, is also characteristic of the oceanic adjustment to the large-scale baroclinic Rossby waves described in Sévellec and Fedorov (2013). EGC changes translate into an increased export of fresher waters into the subpolar gyre, which reverses the sign of the

initial salinity anomalies in the upper Labrador Sea ($S300_{LAB}$). This process is key to sustain the 20-year cycle in the advective mechanism. Here, we have shown that it is convection, the associated changes in subsurface density, and their later impact on the EGC that provide the two-way coupling between the two mechanisms.

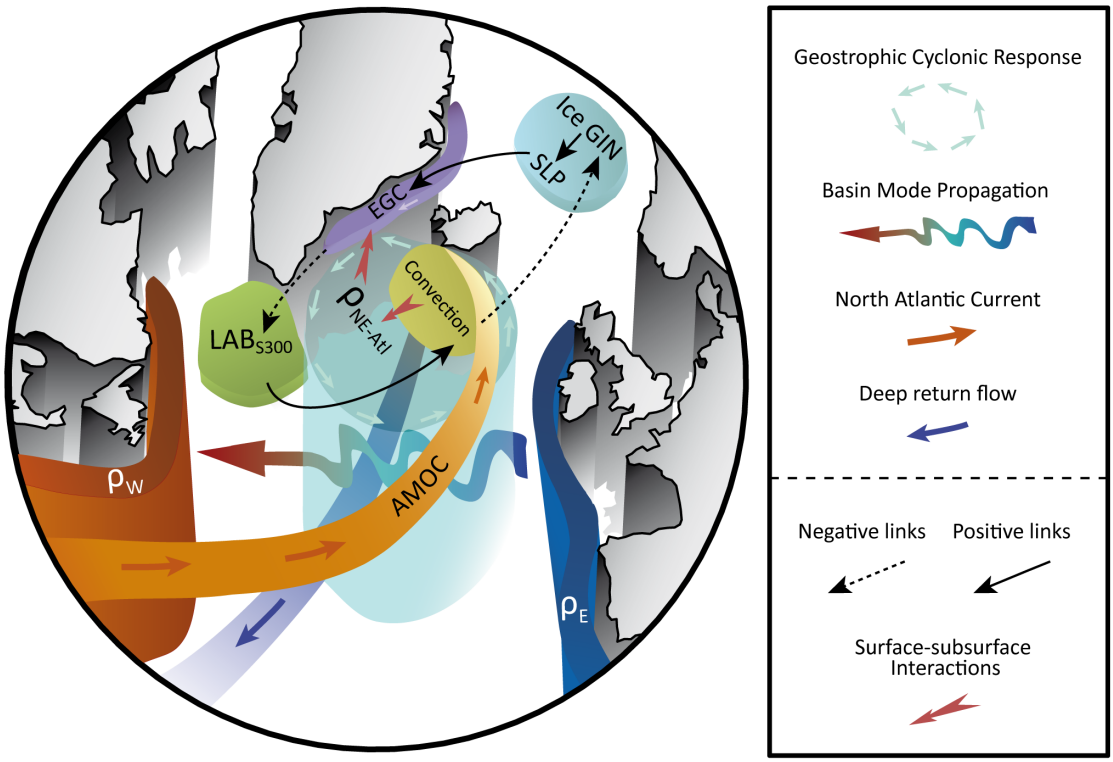

Figure 12: Schematic of the variables and interactions involved in the North Atlantic 20-year cycle in IPSL-CM5A.

Summary and Discussion

To summarize, an updated view of the processes and interactions responsible for the bi-decadal AMOC variability in IPSL-CM5A is provided in the schematic of Figure 12. Until now, AMOC variability in the model was explained through salinity-driven changes in the deep convection regions. By characterizing and including the subsurface basin mode we are now able to explain the process by which convection impacts the AMOC. Furthermore, the two modes can coexist and show the same preferential variability because they have accommodated to interact constructively with each other.

In essence, the whole cycle develops as follows. Upper ocean positive salinity anomalies are advected by the subpolar gyre from the Labrador Sea into the sinking regions south of Iceland (in 5 years), where they enhance deep convection and a negative thermal anomaly is formed from the surface down to 2000 m. This induces a geostrophic response, characterized by a cyclonic flow that propagates westwards in the subsurface as a result of its interaction with the mean meridional density gradient. As the anomalies reach the eastern Greenland coast 2 years after, the associated cyclonic flow leads at the surface to an intensification of the EGC. This effect on the EGC comes on top of the weak feedback mechanism with sea ice and SLP anomalies in the Nordic Seas already described in *Escudier et al. (2013)*, and contributes to synchronize the two multidecadal modes. At depth, density anomalies continue their westward propagation until they reach the Canadian coast 6 years after, propagating southward along the western boundary current, and establishing a strong zonal gradient that triggers a northward thermal wind response, thus strengthening the AMOC. Phase reversal in the upper ocean is related to the EGC, and its export of fresh waters from the Arctic into the subpolar gyre, building up large anomalies in the Labrador Sea 3 years after (10 years if we count from the beginning of the cycle). Accordingly, the phase reversal in the deeper ocean appears when these negative salinity anomalies reach the vicinity of Iceland 5 years later, and debilitate deep convection. Note that at this stage, surface waters over the region are gradually warming, in response to the increase in northward heat transport that follows the strengthened AMOC phase. This suggests that the AMOC plays a preconditioning role in the phase reversal of convection.

Observational records do support a prominent 20-year time scale in the North Atlantic, supported, for instance, by sea level estimates at the east and western boundaries (*Frankcombe & Dijkstra, 2009*), and also in reconstructed estimates of Greenland

temperature (*Chylek et al., 2011*) and the sea ice edge in the Nordic Seas (*Divine & Dick, 2006*). Regarding the specific variables involved in our mechanism, there exist evidence of decadal fluctuations in salinity measurements of the Labrador Sea, shaped by the occurrence of the Great Salinity Anomalies (*Belkin et al., 1998; Swingedouw et al., 2015).* It is not clear, however, if they also present a modulation at 20 years. Only short records for the EGC variability are available, insufficient to assess its multidecadal changes. There is, however, a long proxy record for local SST in its vicinity that exhibits a significant peak at 20 years (*Sicre et al., 2008*). All of the above suggests that some of the features of our mechanism might be realistic. Yet, it is important to keep in mind that some other aspects are inherent to the model and its main biases. For example, one important limitation of IPSL-CM5A and former versions is its inability to represent deep convection in the Labrador Sea, due to too fresh local climatological conditions over the area *(Swingedouw et al., 2007)*. This misrepresentation is probably decisive to allow for the salinity advection mechanism in *Escudier et al. (2013)* and its particular arrangement with the subsurface basin mode. Otherwise, EGC-driven salinity anomalies would first arrive and impact the Labrador region, being partly transformed into a thermal anomaly reaching deeper levels. Hence, it could modify the upper and lower ocean signals being advected by the subpolar gyre and possibly compromise the westward propagation from the region south of Iceland.

Our results nevertheless support the coexistence of a multidecadal subsurface basin mode with an advective mechanism at the surface, and prompts for further investigations in other coupled climate models. In IPSL-CM5A, the westward propagation is excited and sustained by salinity-driven deep convection following surface oscillatory mechanism (Escudier et al., 2013), and not simply by stochastic forcing from the atmosphere like other analyses suggest *(Frankcombe et al., 2009;*

Sévellec et al., 2009). This may explain why the 20-year variability is so pronounced in IPSL-CM5A. Identifying this kind of mechanism in other coupled climate models, with different representations of North Atlantic convection and the AMOC, is essential to ascertain whether the basin mode propagation is actually predominant or if, on the contrary, its signal becomes strongly damped by the influence of the atmosphere. *Tulloch and Marshall (2012)* described a similar mechanism in both CCSM3 and the GFDL Climate Model version 2.1 (CM2.1), involving a westward propagation of subsurface density anomalies in a timescale broadly consistent with the transit of first baroclinic mode Rossby waves, which affects the AMOC through a thermal wind response. Interestingly, in both models a predominant 20-year time-scale for the AMOC was also identified, despite some differences in their upper ocean variability. This suggests that the subsurface basin mode may be the key mechanism to generate bi-decadal AMOC variability, and that it can appear under other coupled model configurations. In the particular case of our study, we have seen that the subsurface basin mode is also compatible with an upper ocean mechanism driven by EGC variations, which share similarities with some of the observed Great Salinity Anomalies *(Swingedouw et al., 2013, 2015)*.

Acknowledgements :

This study was partly funded by the EU project SPECS funded by the European Commission's Seventh Framework Research Programme under the grant agreement 308378, by the MORDICUS Project funded by the Agence Nationale de la Recherche under grant agreement ANR-13-SENV-0002-02, and by the Natural and Environmental Research Council UK (MESO-CLIP, NE/K005928/1). The authors thank Alexey V. Fedorov for fruitful discussions on the topic.

References

Aumont, O., Bopp, L., 2006. Globalizing results from ocean in situ iron fertilization studies. *Global Biogeochemical Cycles*, 20, GB2017.

Belkin, I.M., Levitus, S., Antonov, J., Malmberg, S.-A., 1998. "Great Salinity Anomalies" in the North Atlantic. *Progress in Oceanography*, 41, 1-68.

Bretherton, C. S., Widmann, M., Dymnikov, V. P., Wallace, J. M., Bladé, I., 1999. The effective number of spatial degrees of freedom of a time-varying field, *J Climate*, 12, 1990–2009.

Cheng, W., Bleck, R., Rooth, C., 2004. Multi-decadal thermohaline variability in an ocean-atmosphere general circulation model. *Climate Dynamics*, 22, 573-590.

Chylek, P., Folland, C.K., Dijkstra, H.A., Lesins, G., Dubey, M.K., 2011. Ice core data evidence for a prominent near 20 year time scale of the Atlantic Multidecadal Oscillation. *Geophysical Research Letters*, 38, L13704.

Colin de Verdière, A., Huck, T., 1999. Baroclinic instability: An oceanic wavemaker for interdecadal variability. *Journal of Physical Oceanography*, 29, 893-910.

Cronin, T.M., Farmer, J., Marzen, R.E., Thomas, E., Varekamp, J.C., 2014. Late Holocene sea level variability and Atlantic Meridional Overturning Circulation. *Paleoceanography*, 2014PA002632.

Cunningham, S.A., Kanzow, T., Rayner, D., Baringer, M.O., Johns, W.E., Marotzke, J., Longworth, H.R., Grant, E.M., Hirschi, J.J.-M., Beal, L.M., Meinen, C.S., Bryden, H.L., 2007. Temporal Variability of the Atlantic Meridional Overturning Circulation at 26.5 N. *Science*, 317, 935-938.

Danabasoglu, G., 2008. On Multidecadal Variability of the Atlantic Meridional Overturning Circulation in the Community Climate System Model Version 3. *J Climate*, 21, 5524-5544.

Delworth, T.L., Manabe, S., Stouffer, R.J., 1993. Interdecadal Variations of the Thermohaline Circulation in a Coupled Ocean-Atmosphere Model. *J Climate,* 6, 1993–2011.

Deshayes, J., Frankignoul, C., 2005. Spectral Characteristics of the Response of the Meridional Overturning Circulation to Deep-Water Formation. *Journal of Physical Oceanography*, 35, 1813-1825.

Divine, D. V., Dick, C., 2006. Historical variability of sea ice edge position in the Nordic Seas. *J. Geophys. Res. Ocean*, 111, 1-14.

Dong, B., Sutton, R.T., 2005. Mechanism of Interdecadal Thermohaline Circulation Variability in a Coupled Ocean–Atmosphere GCM. *J Climate,* 18, 1117–1135.

Dufresne, J.L., Foujols, M.A., Denvil, S., Caubel, A., Marti, O., Aumont, O., Balkanski, Y., Bekki, S., Bellenger, H., Benshila, R., Bony, S., Bopp, L., Braconnot, P., Brockmann, P., Cadule, P., Cheruy, F., Codron, F., Cozic, A., Cugnet, D., de Noblet, N., Duvel, J.P., Ethe, C., Fairhead, L., Fichefet, T., Flavoni, S., Friedlingstein, P., Grandpeix, J.Y., Guez, L., Guilyardi, E., Hauglustaine, D., Hourdin, F., Idelkadi, A., Ghattas, J., Joussaume, S., Kageyama, M., Krinner, G., Labetoulle, S., Lahellec, A., Lefebvre, M.P., Lefevre, F., Levy, C., Li, Z.X., Lloyd, J., Lott, F., Madec, G., Mancip, M., Marchand, M., Masson, S., Meurdesoif, Y., Mignot, J., Musat, I., Parouty, S., Polcher, J., Rio, C., Schulz, M., Swingedouw, D., Szopa, S., Talandier, C., Terray, P., Viovy, N., Vuichard, N., 2013. Climate change projections using the IPSL-CM5 Earth System Model: from CMIP3 to CMIP5. *Climate Dynamics*, 40, 2123-2165.

Escudier, R., Mignot, J., Swingedouw, D., 2013. A 20-year coupled ocean-sea ice-atmosphere variability mode in the North Atlantic in an AOGCM. *Climate Dynamics*, 40, 619–636.

Feng, Q.Y., Dijkstra, H., 2014. Are North Atlantic multidecadal SST anomalies westward propagating? *Geophysical Research Letters*, 41, 541-546.

Fichefet, T., Maqueda, M.A.M., 1997. Sensitivity of a global sea ice model to the treatment of ice thermodynamics and dynamics. *Journal of Geophysical Research: Oceans*, 102, 12609-12646.

Frankcombe, L.M., Dijkstra, H.A., von der Heydt, A., 2008. Sub-surface signatures of the Atlantic Multidecadal Oscillation. *Geophysical Research Letters*, 35, L19602.

Frankcombe, L.M., Dijkstra, H.A., von der Heydt, A., 2009. Noise-Induced Multidecadal Variability in the North Atlantic: Excitation of Normal Modes. *Journal of Physical Oceanography*, 39, 220-233.

Frankcombe, L.M., von der Heydt, A., Dijkstra, H.A., 2010. North Atlantic Multidecadal Climate Variability: An investigation of dominant time scales and processes. *J Climate*, 23, 3626-3638.

Gray, S.T., Graumlich, L.J., Betancourt, J.L., Pederson, G.T., 2004. A tree-ring based reconstruction of the Atlantic Multidecadal Oscillation since 1567 A.D. *Geophys. Res. Lett.* 31, 2–5.

Hawkins, E., Sutton, R.T., 2007. Variability of the Atlantic thermohaline circulation described by three-dimensional empirical orthogonal functions. *Climate Dynamics*, 29, 745-762.

Held, I.M., 1983. Stationary and quasi-stationary eddies in the extratropical atmosphere: theory. In B.J.H.a.R.P. Pearce (Ed.), *Large-scale dynamical processes in the atmosphere* (pp. 127--168).

Hirschi, J., Marotzke, J., 2007. Reconstructing the meridional overturning circulation from boundary densities and the zonal wind stress. *Journal of Physical Oceanography*, 37, 743-763.

Hourdin, F., Foujols, M.-A., Codron, F., Guemas, V., Dufresne, J.-L., Bony, S., Denvil, S., Guez, L., Lott, F., Ghattas, J., Braconnot, P., Marti, O., Meurdesoif, Y., Bopp, L., 2013. Impact of the LMDZ atmospheric grid configuration on the climate and sensitivity of the IPSL-CM5A coupled model. *Climate Dynamics*, 40, 2167-2192.

Huck, T., De Verdiere, A.C., Weaver, A.J., 1999. Interdecadal variability of the thermohaline circulation in box-ocean models forced by fixed surface fluxes. *Journal of Physical Oceanography*, 29, 865-892.

Jungclaus, J.H., Haak, H., Latif, M., Mikolajewicz, U., 2005. Arctic–North Atlantic Interactions and Multidecadal Variability of the Meridional Overturning Circulation. *J Climate* 18, 4013–4031.

Killworth, P.D., Blundell, J.R., 2007. Planetary Wave Response to Surface Forcing and Instability in the Presence of Mean Flow and Topography. *Journal of Physical Oceanography*, 37, 1297-1320.

Killworth, P.D., Chelton, D.B., DeSzoeke, R.A., 1997. The speed of observed and theoretical long extratropical planetary waves. *Journal of Physical Oceanography*, 27, 1946-1966.

Kwon, Y.-O., Frankignoul, C., 2014. Mechanisms of Multidecadal Atlantic Meridional Overturning Circulation Variability Diagnosed in Depth versus Density Space. *Journal of Climate*, 27, 9359-9376.

Madec, G., 2008. NEMO ocean engine. *Notes du Pole de Modelisation. Institut Pierre-Simon Laplace (IPSL)*, No 27.

Marshall, J., Scchott, F., 1999. Open-ocean convection: Observations, theory, and models. *Rev. Geophys.* 37,1–64.

Menary, M.B., Park, W., Lohmann, K., Vellinga, M., Palmer, M.D., Latif, M., Jungclaus, J.H., 2012. A multimodel comparison of centennial Atlantic meridional overturning circulation variability. *Climate Dynamics*, 38, 2377-2388.

Mignot, J., Swingedouw, D., Deshayes, J., Marti, O., Talandier, C., Séférian, R., Lengaigne, M., Madec, G., 2013. On the evolution of the oceanic component of the IPSL climate models from CMIP3 to CMIP5: A mean state comparison. *Ocean Modelling*, 72, 167-184.

Ortega, P., Montoya, M., González-Rouco, F., Mignot, J., Legutke, S., 2012. Variability of the Atlantic meridional overturning circulation in the last millennium and two IPCC scenarios. *Climate Dynamics*, 38, 1925-1947.

Persechino, A., Mignot, J., Swingedouw, D., Labetoulle, S., Guilyardi, E., 2013. Decadal predictability of the Atlantic meridional overturning circulation and climate in the IPSL-CM5A-LR model. *Climate Dynamics*, 40, 2359-2380.

Rayner, N., Parker, D., Horton, E., Folland, C.K., Alexander, L., Rowell, D., Kent, E., Kaplan, A., 2003. Global analyses of sea surface temperature, sea ice, and night marine air temperature since the late nineteenth century. *J. Geophys. Res*, 108, 4407.

Rossby, C.G., 1939. Relation between variations in the intensity of the zonal circulation of the atmosphere and the displacements of the semipermanent centers of action. *Journal of Marine Research*, 2, 38-55.

Servonnat, J., Mignot, J., Guilyardi, E., Swingedouw, D., Séférian, R., Labetoulle, S., 2015. Reconstructing the subsurface ocean decadal variability using surface nudging in a perfect model framework. *Climate Dynamics*, 44, 315-338.

Sévellec, F., et al., 2009: Nonnormal multidecadal response of the thermohaline circulation induced by optimal surface salinity perturbations. *J. Phys. Oceanogr.*, 39, 852–872.

Sévellec, F., Fedorov, A.V., 2013. The Leading, Interdecadal Eigenmode of the Atlantic Meridional Overturning Circulation in a Realistic Ocean Model. *Journal of Climate*, 26, 2160-2183.

Sévellec, F., Fedorov, A.V., 2015. Optimal excitation of AMOC decadal variability: Links to the subpolar ocean. *Progress in Oceanography*, 132, 287‑304.

Sévellec, F., Huck, T., 2015. Theoretical investigation of the Atlantic multidecadal oscillation. *Journal of Physical Oceanography,* published online.

Sévellec, F., Huck, T., Ben Jelloul, M., Vialard, J., 2009. Nonnormal Multidecadal Response of the Thermohaline Circulation Induced by Optimal Surface Salinity Perturbations. *J Phys Oceanography*, 39, 852-872.

Schlesinger, M.E., Ramankutty, N., 1994. An oscillation in the global climate system of period 65-70 years. *Nature*, 367, 723–726.

Sicre, M., Jacob, J., Ezat, U., Rousse, S., Kissel, C., Yiou, P., Eiríksson, J., Knudsen, K.L., Jansen, E., Turon, J.-L., 2008. Decadal variability of sea surface temperatures off North Iceland over the last 2000 years. *Earth and Planetary Science Letters*, 268, 137-142.

Swingedouw, D., Braconnot, P., Delecluse, P., Guilyardi, E., Marti, O., 2007. The impact of global freshwater forcing on the thermohaline circulation: adjustment of North Atlantic convection sites in a CGCM. *Climate Dynamics*, 28, 291-305.

Swingedouw, D., Mignot, J., Labetoulle, S., Guilyardi, E., Madec, G., 2013. Initialisation and predictability of the AMOC over the last 50 years in a climate model. *Climate Dynamics*, 40, 2381-2399.

Swingedouw, D., Ortega, P., Mignot, J., Guilyardi, E., Masson-Delmotte, V., Butler, P.G., Khodri, M., Séférian, R., 2015. Bidecadal North Atlantic ocean circulation variability controlled by timing of volcanic eruptions. *Nat. Commun.* 6, published online.

te Raa, L., Dijkstra, H., 2002. Instability of the thermohaline ocean circulation on interdecadal timescales. *Journal of Physical Oceanography*, 32, 138-160.

Timmermann, A., Latif, M., Voss, R., Grötzner, A., 1998. Northern Hemispheric Interdecadal Variability: A Coupled Air–Sea Mode. *J Climate,* 11, 1906-1931.

Tulloch, R., Marshall, J., 2012. Exploring Mechanisms of Variability and Predictability of Atlantic Meridional Overturning Circulation in Two Coupled Climate Models. *J. Climate*, 25, 4067-4080.

Tulloch, R., Marshall, J., Smith, K.S., 2009. Interpretation of the propagation of surface altimetric observations in terms of planetary waves and geostrophic turbulence. *Journal of Geophysical Research-Oceans*, 114, C02005.

Vellinga, M., Wu, P., 2004. Low-Latitude Freshwater Influence on Centennial Variability of the Atlantic Thermohaline Circulation. *J Climate,* 17, 4498-4511.

Venegas, S.A., Mysak, L.A., 2000. Is there a dominant timescale of natural climate variability in the Arctic? *Journal of Climate*, 13, 3412-3434.

Vianna, M.L., Menezes, V.V., 2013. Bidecadal sea level modes in the North and South Atlantic Oceans. *Geophysical Research Letters*, 40, 5926-5931.